Global NEST Journal, Vol 25, No 5, pp 1-10

Adsorption of cationic dye (Red 95) from aqueous solution by biosynthesized nano particle of cumnium cyminum

Rajeshkumar V.[1], Senthil Kumar M.[2], Al-Zaqri N.[3] and Boshaala A.[4,5]

[1]Department of Civil Engineering, KPR Institute of Engineering and Technology, Arasur- 641 407, Coimbatore, Tamil Nadu, India

[2]Department of Environmental Engineering, College of Engineering and Technology, Bule Hora University, Bule Hora, West Guji, Ethiopia

[3]Department of Chemistry, College of Science, King Saud University, P.O. Box- 2455, Riyadh 11451, Saudi Arabia

[4]Research Centre, Manchester Salt & Catalysis, Unit C, 88-90 Chorlton Rd, M154AN Manchester, United Kingdom

[5]Libyan Authority for Scientific Research, P.O. Box 80045, Tripoli, Libya

Received: 19/01/2023, Accepted: 31/01/2023, Available online: 01/02/2023

*to whom all correspondence should be addressed: e-mail: rajeshcit16@gmail.com

https://doi.org/10.30955/gnj.004749

Graphical abstract

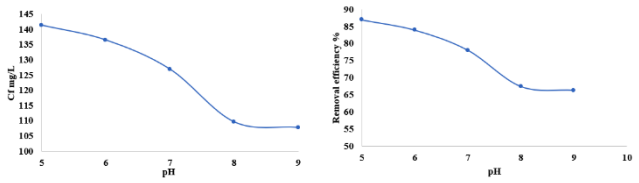

Abstract

In the present work, the potential of cumnium cyminum as an effective bio adsorbent for the removal of cationic dye (Red 95) was investigated. Batch adsorption experiments were carried out to investigate the effects of adsorbent dosage, pH and contact time with initial dye concentration on adsorption. In connection with adsorbent dosage the highest removal efficiency was 143.64mg/L of removal efficiency 88.36%, regarding pH study the peak removal attained with 141.37mg/L with the removal percentage 86.76% and for contact time study the removal efficiency attained in the concentration of 142.10mg/L in the removal percentage of 87.41%. The adsorption studies demonstrated that the Thomson model, and Yoon nelson model are excellent descriptions of adsorption processes. The maximum adsorption capacity of 143.64 mg/L toward biosynthesized nano adsorbent with removal rates of 88.36% and greatest R^2 value of around 0.9879 was well suited to the equilibrium data. The ANOVA was used for the analysis of variance to determine the best parameters for the overall adsorption model. Utilizing SEM, XRD, and FTIR methods, the adsorbent was characterized. Different desorbing agents, such as NaOH, HCl, and NaCl, were examined for the desorption of cationic dye (Red 95) loaded with adsorbent generated from cumnium cyminum, and it was shown that HCl was the most effective desorbing agent when combined with deionized doubly distilled water (DDDW). The proportion removal of cationic dyes was improved with increasing adsorbent dose and contact time and the percent of color exclusion was decreasing with increasing pH.

Keywords: Adsorption, cationic dye (red 95), biosynthesize, desorption

1. Introduction

In recent years, a variety of industries, including food technology, pharmaceuticals, the cosmetics industry, and the dyeing of leather and textiles, have made extensive use of dyes and pigments (Davarci *et al*., 2023). 100 tons of dyes are thought to be released into the environment each year by the dyeing industry, damaging springs and rivers. The lengthy process sequence that results in large waste production throughout the textile manufacturing process is characterized by the high consumption of resources like water and a variety of chemical dyes (Zhu *et al*., 2023). Environmental protection is becoming increasingly concerned with how spent dye effluent is treated. Because dyes are hazardous and unpleasant, difficulties arise when wastewater from these companies is discharged into water resources (Vahedi*et al*., 2017). Due to their synthetic origin, very complex molecular structure, and durability built to endure destruction by light, chemical, biological, and other causes, dyes are difficult to remove once they have meet water (Zhang *et al*., 2014). They are highly challenging to deteriorate as a result. Most dyes, particularly cationic dyes, have been found to be poisonous, mutagenic, carcinogenic, and even pose a substantial risk to aquatic life and people (Yang *et al*., 2020). Environmental protection and wastewater treatment are seriously hampered by the discharge of wastewater containing colours into bodies of water and ground water. Additionally, dyes block light from entering, which lowers the amount of photosynthetic activity in water streams and disturbs the balance of the aquatic ecosystem (Yun *et al*., 2020). There is not a single,

effective way to get rid of dye effluents. The type of dyes to be eliminated, their composition, concentrations, and production flow into the wastewater all influence the optimum option (Shi *et al*., 2019). A variety of physical, chemical, and biological techniques have been researched to remove dyes from aqueous solutions. Consequently, colour removal from dyeing effluent is very difficult one (Senoussi *et al*., 2018). For the removal of dyes from wastewater, several approaches have been used, including adsorption, oxidation, flocculation, biodegradation, ion-exchange, electrolysis, and photo catalysis (Lapwanit *et al*., 2018). Adsorption has drawn the most attention among the many approaches based to its many benefits in the aspect of price, convenience of use, suppleness, and easiness of project, as well as its insensitivity to harmful contaminants (Zhou *et al*., 2018). Activated carbon, biosynthesized materials, synthetic materials, and surface-modified materials including lignite, kaolinite, and silica materials are only a few examples of the various adsorbents helped to eliminate dye (Zereshki *et al*., 2018). Owing to their affordability, comfort of use, biodegradability, biocompatibility, and renewability, adsorbents made from agricultural by-products have gained growing interest over the past few years (Hosseinzadeh *et al*., 2018). Biosynthesized materials were chosen as an adsorbent in this investigation due to their simplicity and effectiveness in the study through literature review (Wang *et al*., 2022). This work concentrated on the removal of cationic dye (Red 95) by an adsorption procedure that used cumnium cyminum as an adsorbent in the biosynthesize approach (Abrishamkar *et al*., 2023). Investigations have been done into the impacts of contact time, starting dye attentiveness, adsorbent dosage, pH, and temperature (Wang *et al*., 2017). Using the Thomson model, and the Yoon nelson model, the kinetics of adsorption and maximum adsorption capacity were also investigated (Isanejad *et al*., 2017). Using the analysis of variance by ANOVA the ideal parameters for the complete adsorption model were discovered. Following the adsorption procedure, the physicochemical characteristics of the biosynthesized cuminium cyminum adsorbent were assessed by X-ray diffraction (XRD), scanning electron microscopy (SEM), and fourier transformation infrared spectrum (FT-IR) (Tao *et al*., 2023). The resin's ability to be reused and its adsorption capability were both examined to increase its economic use (Kim *et al*., 2023). The desorption was performed using a variety of chemicals, including NaOH, HCl, and NaCl, and the outcomes shown in this research can offer a simple, affordable method for rapid separation performance in aqueous medium while also making diverse cationic dyes easy to remove.

2. Materials and methods

2.1. Materials

The chemicals for experimental study purchased in a research scale cationic dye (Red 95) (Fucai chem), HCl (ReAgent chemicals), NaOH (Lab Alley) and NaCl (Flinn) were used in the present investigation. Deionization and double distillation were employed for the experimental study.

2.2. Preparation adsorbent

Cuminium cyminum was acquired and it is cleaned thoroughly by double distilled water to remove unwanted particles present in the external portion by desiccated in the sun for about 24hours before being accelerated in an air oven at 80°C for 12 hr (Kadhom *et al*., 2020). A mechanical grinder was used to turn the dried bulk into a fine powder, which was then sieved through 90 BSS mesh. Then, it was thoroughly cleaned with DDDW to get rid of all the color and turbidity from previous washings (Lin *et al*., 2020). Finally, the cleaned adsorbent was dried for roughly 3 hours at 100°C in an air oven. After drying, the mass was once more crushed, separated into different fractions using a set of sieves, and then kept in airtight containers (Ji *et al*., 2019). Characterization done with the help Scanning electron microscopy (SEM), X-ray diffraction and FTIR were used to examine the surface morphology of the biosynthesized adsorbent both before and after adsorption.

2.3. Batch mode adsorption

The batch adsorption experiments were carried out at room temperature by stirring weighed amounts of the adsorbent in 100 ml of colour dye solutions at the required pH, contact time, initial concentration, and dose of the adsorbent (Yu *et al*., 2019). Dye solution with a agitate speed of 250 rpm for 5h. These experiments were conducted in various 250 ml flasks. The quantity of adsorbent applied to each flask was first calculated. After shaking the sample were taken and filtered by membrane filter paper of pore size 250µm (Qingwen *et al*., 2027). The solution pH was adjusted using HCl or NaOH solutions. The concentration of dye in the solutions was determined spectrophotometrically using the UV-visible spectrophotometer method in each experiment, which was repeated twice (Kono *et al*., 2017). The amount of dye adsorbed per unit mass of resin was calculated from the following expression:

$$q_e = \left(C_0 - C_e\right) x\ V / \left(m\right)$$

Where qe (mg/g) was the adsorbent capacity, C_o, and C_e (mg/L) were the initial and equilibrium dye concentrations in the aqueous solution; V (ml) was the volume of the experimental solution and m (g) was the weight of adsorbent.

2.4. Kinetic study

2.4.1. Thomson model

Using the Thomson model, the relationship between the inner and outer adsorption progressions was revealed (Cui *et al*., 2019). Equation can be used to express the Thomson model.

$$ln\left(\frac{Co}{Ct} - 1\right) = kTH\ qeW\ -\ kTH\ Co\ t \qquad (1)$$

kTH is the Thomson rate constant (ml/min.mg), where qe is the adsorption capacity, Co is the inlet ion

concentration, Ct is the effluent ion concentration at time t (mg/L), W is the mass of the adsorbent (g), Q is the inlet flow rate (ml/min), and t is the flow time t. (min). The value of Co/Ct is the ratio of the ion concentrations at the intake and outflow. Squeezing ln (Co/Ct-1) against time yielded the values of qe and kTH from the interference point and slope of the plot, respectively (t).

2.4.2. Yoon nelson model

The Yoon-Nelson Model does not require extensive proof of the adsorbate, it is more straightforward. According to this model, the chance of adsorption for each adsorbate fragment decreases in a manner that is proportional to both the chance of adsorbate and the potential for adsorbate revolution on the adsorbent (Xu *et al*., 2018). It is a typical for a single element system, the linearized equation of model expressed as Eq:

$$ln\frac{Ct}{Co-Ct} = kyt - tky \quad (2)$$

where (min) is the minimum time necessary for 50% adsorbate breakthrough and kyt (min-1) is the rate constant. Model by Yoon and Nelson linear plots. The interrupt and grade of the ln [Ct/C0-Ct] vs. t graph's linear design can be used to derive the parameters ky.

2.5. ANOVA analysis

An experiencing collective contradiction created from special statistics developed is divided into systematic rudiments and arbitrary aspects using the examination of variance (ANOVA) method of statistical analysis (Yuan *et al*., 2019). It starts the stimulation that an unnamed autonomous object has on a dependent variable in a regression analysis. Using a one-way ANOVA, the connection among the dependent and independent variables in this study is conclusively demonstrated (Wu *et al*., 2019). The substantial amount of outcome level of effective parameters on response have frequently been controlled using the ANOVA method. This method is applied in this study to motivate the mean square competency of each parameter, and the calculation outcomes are examined (Bensalah *et al*., 2017). The sum of squares (SS), degree of freedom (DF), mean of squares (MS), F values, and effect ratios of each parameter are calculated using the ANOVA method. Common techniques for doing this include cross confirmation, testing, and assessment (Farhadi *et al*., 2017). The foundation for calculating testing is made up exclusively of testing model but in physical research, this is frequently not likely because there are conventionally insufficient instances (Pradhan *et al*., 2020). Then, an improved method is labouring, which tries to do travesty prediction testing by constantly removing possessions from the data assortment.

2.6. Material characterization

The X-ray diffraction (XRD) measurements were collected using a Scientific XLR Scientech Y'XLR diffractometer between 3° and 90° (3θ) with a scanning rate of 0.2°/s, employing Cu Kα radiation (λ = 1.68451 Å) (Wang *et al.*, 2020). The nature of surface species was determined by Fourier transform infrared spectroscopy (FT-IR). The FT-IR spectra were recorded using an Empyrean SSM-990 spectrometer in Cur pellets (Gajera *et al*., 2022). The samples were combined with CUr, dried at 220 °C, and then subjected to infrared light. After processing, the pellets were measured immediately in the mid-infrared region under ambient lighting. Averaging 64 images at wavelengths between 6000 and 600 cm-1 produced the spectra (Lv *et al*., 2022). At a liquid nitrogen temperature of 80 K, the adsorption-desorption isotherms were measured using a nitrogen adsorption system (Scientech MPN1024). Thermogravimetric method followed by Settler Arithmetic thermos prism.TG/DTG curves were recorded with a 20 °C/min heating rate under air atmosphere (70mL·min−1) between 60 and 800°C (Xu *et al*., 2019). Scanning electron microscopy (SEM) analysis was directed using an Alpha Z-6800 electron microscope. Individual sample was mounted on an aluminum stub and given a gold coating for the SEM tests.

2.7. Desorption study

Using the solvent desorption method, exhausted adsorbent that had been saturated the Cationic dye effluent again adsorbent was rejuvenated (Wang *et al.*, 2019). An external filtration procedure was used to separate the resin following adsorption equilibrium. The desorption trials were supported by batch with different reagents such as 0.1 M HCl, 0.1 M NaOH and 0.1 M NaCl and water (Wang *et al.*, 2019). The adsorbent was treated with double distilled water. To get rid of any remaining dye that had not been absorbed (Yang *et al.*, 2018). The dye-loaded adsorbents were stirred for 5 hours with 30 mL of various desorbing solutions.

3. Result and Discussion

3.1. Batch adsorption study

The aqueous sample was prepared for the concentration of 162.56mg/L to assess the initial concentration of dye gated at a maximum peak at 650 nm of wavelength at 4.0 absorbance of an ultraviolet-visible spectrophotometer (Zhiming *et al.*, 2017). The cationic dye (Red 95) available in concentrated sample, it was most effective to form the colour of aqueous sample. To determine the adsorption efficiency, the adsorbent was used in different concentrations against dye solutions, the dye was prepared based on the intensity of the dye colour and compassion of the instrument for the dye variety (Janus *et al.*, 2019). The wavelengths of maximum absorbance (λ max) of the solutions were determined for the dye and calibration curves are constructed to determine the initial and final concentration. Then the next sequence of solutions made by corresponding volume of the previously concentrated dye solutions using distilled water and measuring their absorbance at their respective λmax. The calibration curve designed based on the concentration and measured absorbance (Gui *et al*., 2019). The maximum absorption wavelength (650 nm) was used to determine the dye concentrations. A calibration curve was obtained for five different concentrated adsorbents, using samples of known dye concentration of cationic dye (Red

95) (162.56 mg/L), and based on Lambert Beer's law, calibration curves are made (Gajera *et al.*, 2022). From the curves by interpolation or extrapolation, depending on the sample, unknown concentrations of textile wastewater were obtained.

3.1.1. Adsorption study in different concentrated adsorbent

The detailed investigation done to identify the relationship of initial dye concentrations, concentration of adsorbent and percentage removal (Huon *et al.*, 2020). The initial dye concentrations (Ci) 162.56 mg/L at constant pH 6 the dye adsorption was carried out at, contact time 100 minutes. The first concentration 50mg/L of adsorbent attained the percentage removal efficiency of 64.73% with the concentration 105.23mg/L. next adsorbent concentration was 100mg/L attained the removal percentage of 71.81% in the concentration of dye 116.75mg/L, in 150mg/L of adsorbent attained 75.94% of removal efficiency in the concentration range of 123.46mg/L. The next adsorbent in the range of 200mg/L achieved the removal percentage of 88.36% with the concentration of 143.64mg/L. The final concentration of adsorbent was 250mg/L attained the removal percentage of 85.56% which denoted sudden fall in removal with the concentration of 139.10mg/L. This study proved that increasing concentration for optimum level of adsorbent increased the removal efficiency which was showed in Table 1 respectively (Figure 1).

Table 1. Cationic dye (Red 95) removal in different concentrated adsorbent

Concentration of Adsorbent mg/L	C_i (mg/L)	C_f (mg/L)	Removal efficiency (%)
50	162.56	105.23	64.73
100	162.56	116.75	71.81
150	162.56	123.46	75.94
200	162.56	143.64	88.36
250	162.56	139.10	85.56

Table 2. pH variation study in cationic dye (Red 95) adsorption

pH	C_i (mg/L)	C_f (mg/L)	Removal efficiency (%)
5	162.56	141.37	86.96
6	162.56	136.51	83.97
7	162.56	126.92	78.07
8	162.56	109.63	67.43
9	162.56	107.82	66.32

Table 3. Determination of contact time variation in cationic dye (Red 95) adsorption

Contact time (min)	C_i (mg/L)	C_f (mg/L)	Removal efficiency (%)
10	162.56	116.33	71.56
20	162.56	125.51	77.20
30	162.56	137.46	84.55
40	162.56	142.10	87.41
50	162.56	135.62	83.42

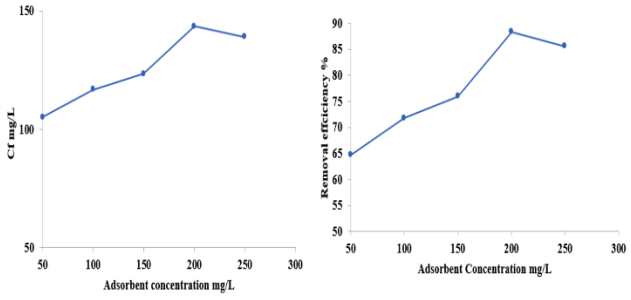

Figure 1 Adsorbent study with removal efficiency

3.1.2. Impact of pH variation in adsorption study

The interrelationship of pH with dye removal efficiency was studied in this process. The HCl solution was used to adjust the pH, the concentration of sample was 162.56mg/L, the pH adjusted for 5 and the absorbance indicated the removal efficiency percentage of 86.96% with the concentration of 141.37mg/L. For pH 6 the removal efficiency got sudden decrease of about 83.97% with the concentration of 136.51mg/L. In the next level the pH 7 attained the removal efficiency of 78.07% with the concentration of 126.92mg/L, the fourth pH range 8 attained the removal percentage of 67.43% in the range of 109.63mg/L. Final pH level was 9 with the removal percentage of 66.32% in the concentration range 107.82mg/L (Li *et al.*, 2018). Table 2 showed that increasing pH with adjusting method decrease the efficiency of dye removal which indicated Figure 2.

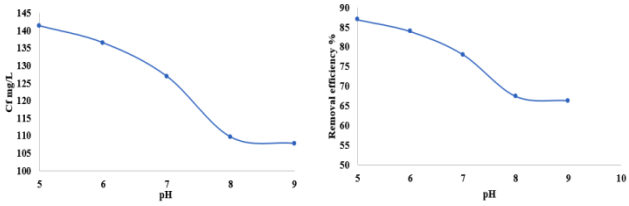

Figure 2 pH variation with removal efficiency

3.1.3. Contact time

The study of contact time in the removal of cationic dye (Red 95) was investigated in this study. The initial concentration (C_i) of dye used for this study is same

162.56mg/L. The contact time of adsorbent varied and the removal efficiency was determined. The contact time 10,20,30,40 and 50 mins was maintained for this study (Xu *et al.*, 2019). For 10min contact time the removal of dye percentage was 71.56% in the concentration of 116.33, in 20min contact time the removal percentage was 77.20% with the concentration of 125.51mg/L. For 30min contact time the percentage of removal was 84.55% with the concentration of 137.46mg/L. The contact time 40min attained the removal percentage range of 87.41% in the dye concentration of 142.10mg/L. For 50min contact time the removal efficiency was 83.42% with the concentration of 135.62mg/L. In 50 min contact time can observe sudden decrease in the dye removal, it denoted that optimum contact time for cationic dye (Red 95) removal for 50min for this study which is indicated in Table 3 and Figure 3 respectively.

3.2. Thomson model

3.2.1. Adsorbent study

Regarding experimental study related to increasing adsorbent dosage from 50mg/L to 250mg/L which is calibrated with the help of Thomson model. It was noted that the inflow concentration (C_i) was uniformly maintained constantly (Ghaemi *et al.*, 2018). The Thomson rate constant caused variation in the kTH at the same time, the kTH value was influenced by the efficiency of removal. The fall of kTH in the range of 0.058 to 0.537 mL/min.mg for a concentration of 162.56 mg/L. While the qe maintained in the range from 0.42 to 12.41 mg/g, the variation in the range was identified. The greater driving force of the inflow concentration may be the cause of this. R^2 was 0.941 and 0.982 which explained in Table 4 respectively.

Table 4. Thomson model of adsorbent variation for cationic dye (Red 95) adsorption

Adsorbent Concentration (mg/L)	50	100	150	200	250
q_e (mg/g)	12.41	18.87	0.987	0.42	11.50
k_{TH} (mL/min.mg)	0.058	0.008	0.41	0.537	0.064
R^2	0.941	0.963	0.971	0.982	0.959

Table 5. Thomson model of pH variation for cationic dye (Red 95) adsorption

pH	5	6	7	8	9
q_e (mg/g)	0.54	0.845	10.42	17.76	9.28
k_{TH} (mL/min.mg)	0.318	0.19	0.062	0.011	0.013
R^2	0.981	0.954	0.912	0.907	0.863

Table 6. Thomson model of contact time for cationic dye (Red 95) adsorption

Contact Time (min)	10	20	30	40	50
q_e (mg/g)	11.50	18.87	0.987	0.42	10.32
k_{TH} (mL/min.mg)	0.068	0.008	0.38	0.450	0.072
R^2	0.947	0.916	0.955	0.981	0.948

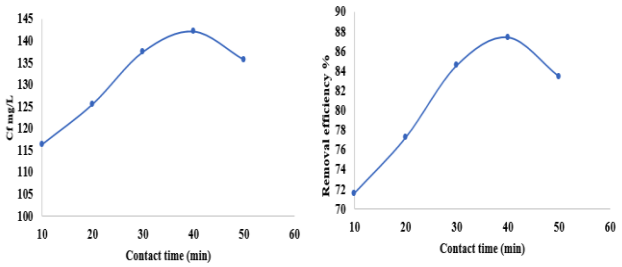

Figure 3. Contact time variation with removal efficiency

3.2.2. pH study

The determination of pH adjustment in the adsorption study was calculated by Thomson model. Regarding experimental study related to increasing pH level by HCl solution in the range from 5 to 9. It denotes that the inflow concentration (C_i) was uniformly maintained constantly (He *et al.*, 2022). The change in the kTH value was influenced by the efficiency of removal which is showed from 0.011 to 0.318 mL/min.mg for a concentration of 162.56 mg/L. While the qe maintained in the range from 0.54 to 17.76 mg/g, the variation in the range was identified. The greater driving force of the inflow concentration may cause decreasing pattern in R^2 value from 0.981 and 0.863 it was reported in Table 5 respectively.

3.2.3. Contact time

The study related to contact time of adsorbent was intended by Thomson model. Concerning with experimental study related to increasing pattern of contact time was determined to study the optimized time of adsorption. The contact time maintained from 10 to 50. It denotes that the inflow concentration (C_i) was uniformly maintained constantly (Ma *et al.*, 2019). The change in the kTH value was influenced by the efficiency of removal. The kTH fell from 0.008 to 0.450 mL/min.mg for a concentration of 162.56 mg/L. While the qe maintained in the range from 0.42 to 18.87 mg/g, the variation in the range was identified. The greater driving force of the

inflow concentration may cause increasing pattern up to 40mins and in 50 mins it denoted the fall in removal efficiency with R^2 value from 0.916 and 0.981 it was reported in Table 6 respectively.

3.3. Yoon Nelson model

3.3.1. Adsorbent study

Based on the values of the regression coefficients, the Yoon-Nelson model confirmed that it was compatible with variation adsorbent concentration. The results showed that cationic dye (Red 95) had a stronger adsorption break through with an R^2 value 50mg/L was 0.9547, for the concentration of 100mg/L the R^2 value of 0.9601, in the adsorbent concentration 150mg/L had an R^2 value of 0.9763, and for 200mg/L had an R^2 value of 0.9851 and in 250mg/L adsorbent R^2 was 0.9750. The rate constant values in the row of adsorbent in various concentration were 2.11, 2.45, 2.73,2.94 and 2.76 from 50-250mg/L of adsorbent ranges respectively (Liu *et al.*, 2018). The Ky(min^{-1}) is 0.472, 0.501, 0.534,0.550 and 0.542. This said that the experimental results were nearly entirely determined by the kinetic values of cationic dye (Red 95) adsorption in different adsorbent ranges which was explained in Tables 7–10 and Figure 4 respectively.

Table 7. Yoon nelson model of adsorbent concentration for cationic dye (Red 95) adsorption

Adsorbent Concentration (mg/L)	Concentration of cationic dye (Red 95)	Ky(min^{-1})	τ(hr)	R^2
50	162.56	0.472	2.11	0.9547
100	162.56	0.501	2.45	0.9601
150	162.56	0.534	2.73	0.9763
200	162.56	0.550	2.94	0.9851
250	162.56	0.542	2.76	0.9750

Table 8. Yoon nelson model of Various pH for cationic dye (Red 95) adsorption

pH	Concentration of cationic dye (Red 95)	Ky(min^{-1})	τ(hr)	R^2
5	162.56	0.412	3.46	0.9541
6	162.56	0.409	3.32	0.9432
7	162.56	0.384	2.89	0.9114
8	162.56	0.375	2.63	0.9075
9	162.56	0.352	2.54	0.9021

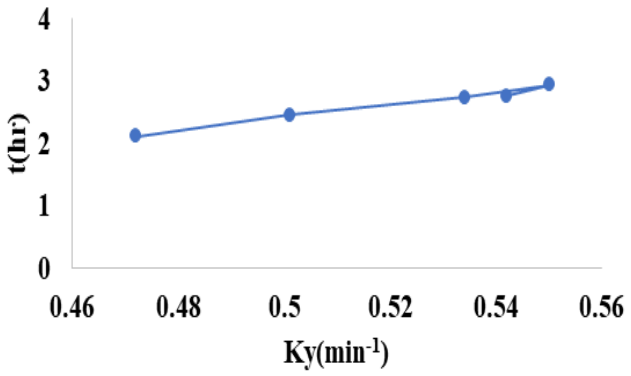

Figure 4. Yoon nelson model for adsorbent variation

3.3.2. pH study

The Yoon-Nelson model confirmed that it was compatible increasing pH range. The results showed that cationic dye (Red 95) had a stronger adsorption break through with an R^2 value 50mg/L was 0.9547, for pH 5 the R^2 value of 0.9541, in pH 6 had an R^2 value of 0.9432, and for pH 7 had an R^2 value of 0.9114 and in pH 9 adsorbent R^2 was 0.9021. The rate constant values in the row of adsorbent in various concentration were 3.46, 3.32, 2.89,2.63 and 2.54 from 5-9 of pH ranges respectively. The Ky(min^{-1}) is 0.472, 0.501, 0.534,0.550 and 0.542 (Hou *et al.*, 2020). This said that the experimental results were nearly entirely determined by the kinetic values of cationic dye (Red 95) adsorption in different adsorbent ranges which was explained in Table 8 and Figure 5 respectively.

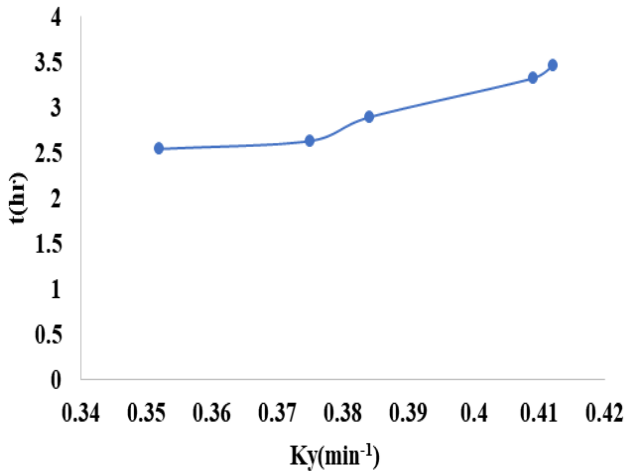

Figure 5. Yoon Nelson model for pH variation

3.3.3. Contact time

The Yoon-Nelson model confirmed that it was compatible increasing contact time of adsorbent. The results showed that cationic dye (Red 95) had a stronger adsorption break through with an R^2 value 10min was 0.9743, for 20min the R^2 value of 0.9769, in 30min an R^2 value of 0.9817, and for 40min had an R^2 value of 0.9833 and in 50min adsorbent R^2 was 0.9751 (Nasiri and Arsalani, 2018). The rate

constant values in the row of adsorbent in various concentration were 1.97, 2.16, 2.65,2.93 and 2.74 from 10-50min of contact time ranges respectively. The Ky(min^{-1}) is 0.425, 0.451, 0.480,0.493 and 0.484. This said that the experimental results were nearly entirely determined by the kinetic values of cationic dye (Red 95) adsorption in different adsorbent ranges which was explained in Table 8 and Figure 6 respectively.

Table 9. Yoon nelson model of contact time variation for cationic dye (Red 95) adsorption

Contact time (min)	Concentration of cationic dye (Red 95)	Ky(min^{-1})	τ(hr)	R^2
10	162.56	0.425	1.97	0.9743
20	162.56	0.451	2.16	0.9769
30	162.56	0.480	2.65	0.9817
40	162.56	0.493	2.93	0.9833
50	162.56	0.484	2.74	0.9751

Table 10. Analysis variance; ANOVA for Quadratic model

Source	Sum of Squares	df	Mean Square	F-value	p-value	Remarks
Model	570.09	15	50.01	618.81	< 0.0001	Significant
A-Initial Concentration	254.35	1	344.35	4168.81	< 0.0001	Significant
B-PH Solution	113.83	1	113.83	1446.53	< 0.0001	Significant
C-Contact Time	33.44	1	33.44	404.01	< 0.0001	Significant
D-Adsorbent Dosage	93.10	1	93.10	1177.71	< 0.0001	Significant
AB	0.9464	1	0.9464	11.98	0.0047	-
AC	4.03	1	4.03	40.26	< 0.0001	Significant
AD	4.48	1	4.48	46.11	< 0.0001	Significant
BC	5.31	1	5.31	56.84	< 0.0001	Significant
BD	0.1124	1	0.1124	2.33	0.3452	-
CD	3.92	1	3.92	38.92	< 0.0001	-
A^2	55.55	1	55.55	708.37	< 0.0001	Significant
B^2	24.99	1	24.99	321.10	< 0.0001	Significant
C^2	34.05	1	34.05	438.60	< 0.0001	Significant
D^2	13.88	1	13.88	177.00	< 0.0001	Significant
Residual	2.16	16	0.0871	-	-	-
Lack of Fit	0.6021	11	0.0602	0.4836	0.9136	not significant
Pure Error	0.7545	6	0.1409	-	-	-
Cor Total	661.25	30	-	-	-	-

3.4. Analysis variance; ANOVA for quadratic model

The model is recommended to be substantial by the Model F-value of 618.81. An F-value this great capacity to owing the range only 0.01% of the time. Where model relations are substantial when the P-value is less than 0.0500. A, B, C, D, AB, AC, AD, BC, CD, A^2, B^2, C^2, and D^2 are not momentous when the range is higher than 0.1000. The reduction range had developed lot of unnecessary terms. The F-value for the lack of fit, 0.6021, denoted the nonexistence is not substantial in contrast to the untainted blunder. The lack of Fit is important in F-value because the value ranged in 91.75% unintended of being caused by noise. Positive is a minor lack of fit (Li *et al.*, 2018). The discrepancy between the Predicted R^2 of 0.9914 and the Adjusted R^2 of 0.9950 is less than 0.003, indicating a fair agreement. This study showed that a good Precision measurement considers the signal-to-noise ratio. A ratio of at least 5 is preferred. An acceptable signal is indicated by the ratio of 88.36. This model can be used to navigate the design space.

3.5. Characterization of adsorbent

3.5.1. SEM analysis

SEM analysis was used to compare the structural characteristics and exterior properties of biosynthetic adsorbent tasters formerly and subsequently cationic dye (Red 95) adsorption (Nayunigari *et al.*, 2017). The results are shown in Figure 7. This demonstrates that the untreated adsorbent's surface is uneven and comprises apertures of various magnitudes and forms, providing a significant exterior area for cationic by-surface interface. However, the dye-loaded adsorbent exterior depicted in Figure 7, it demonstrated that the adsorbent surface was saturated and completely covered by cationic dye.

3.5.2. FTIR study

The occurrence of various functional groups on the surface of the biosynthesized adsorbent was displayed by using FTIR spectroscopy. The FTIR analysis of samples earlier and afterward adsorption was shown in Figure 8 (Shimizu *et al.*, 2022). The band at 4500 cm^{-1} may be caused by the amine group's O-H stretching. The unstable and stable widening of the C-H bond clusters may be the cause of the band at 3421cm^{-1}. The extension of carboxylic acid C=O Strong and sharp group near 2883 cm^{-1} is due to C=O extending. The range of 2835 cm^{-1} and 1633 cm^{-1} in the cationic dye-loaded adsorbent shows that the hydroxyl cluster and carboxyl groups, respectively, it is involved in interacting with the cationic dye (Red 95) during adsorption. Other frequencies also show a small variation in the adsorbent morphology.

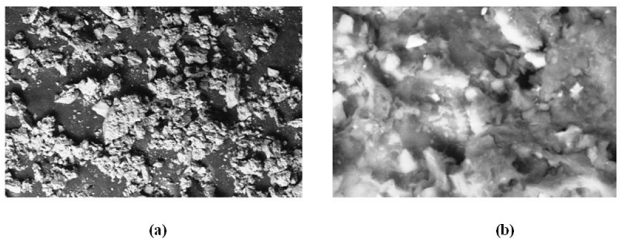

Figure 7. SEM image of adsorbent before(a) and after(b) adsorption study

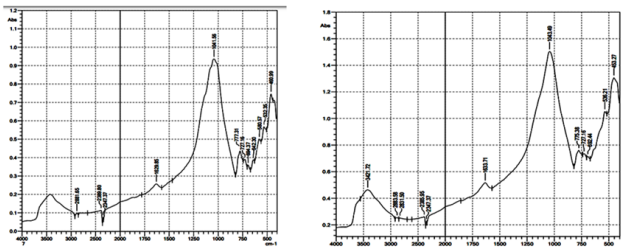

Figure 8. FTIR image of adsorbent before(a) and after(b) adsorption study

3.5.3. XRD analysis

The typical XRD pattern of the biosynthesized adsorbent generated from cumnium cyminum is depicted in Figure 9. Adsorbent is shown both before and after being adsorbed with cationic dye (Red 95). The cubic phase of the adsorbent with a lattice constant of 5.5846 nm was in good agreement with all the diffraction peaks of the cationic dye sample (Priya, 2020). The reflections of the adsorbent's planes were attributed to the peaks at 3 values of 30.47°, 37.58°, 53.35°, 71.48°, and 83.62°, respectively. Other contaminants such metal Na and OH groups were found. The ratio of cationic dye (Red 95) adsorption demonstrated that the biosynthesized adsorbent work out against cationic dye removal because the strong and sharp diffraction peaks revealed the good crystallinity of the adsorbent.

3.6. Desorption study

Desorption experiments with various desorbing agents were conducted to examine the potential for regeneration of utilized biosynthesised adsorbent generated from Cumnium cyminum (0.1 M HCl, 0.1 M NaCl, and 0.1 M NaOH) (Hasanpour and, 2020). The proportion of desorption efficiency was various reagents using Cationic dye (Red 95)-loaded adsorbents is displayed in Table 11 below. With a desorption rate of 41.26%, it revealed that HCl is an improved desorbing agent than other reagents NaCl and NaOH, whose desorption rates were each around 24.57 and 6.83%.

Table 11. Percentage desorption of cationic dye (Red 95) in Cumnium cyminum adsorbent

Desorption Reagent	% Desorption
0.1 M HCl	41.26
0.1 M NaCl	24.57
0.1 M NaOH	6.83

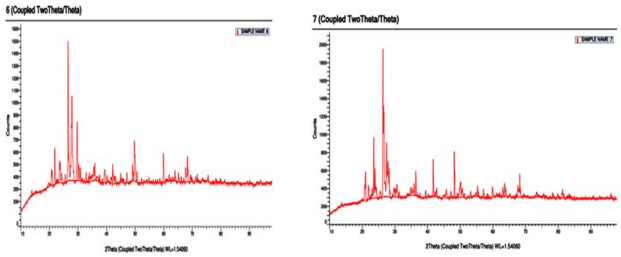

Figure 9. XRD image of adsorbent before(a) and after(b) adsorption study

4. Conclusion

The effectiveness of a biosynthesized adsorbent made from Cuminum cyminum for removing cationic dye (Red 95) was examined in the current work. It discovered that adsorption was influenced by several factors, including initial dye concentration, contact time, pH, and adsorbent dosage. The study discovered that the optimum dosage was 200mg/L. Regarding pH variation experiments revealed that the adsorption capacity increases when the adsorbent is in acidic condition. The equilibrium time for the adsorption of cationic dye (Red 95) onto Cuminum cyminum was found to be 40min.Kinetic study showed that the adsorption process follows Thomas model and Yoon nelson model with R^2 value of around 0.9879 well suited with equilibrium data. Regarding ANOVA There is a 91.75% chance that a Lack of Fit F-value this large could occur due to noise. The Predicted R^2 of 0.9914 is in reasonable agreement with the Adjusted R^2 of 0.9950, It was discovered that the adsorption experiment was endothermic and due to conditional aspect, there is an intensification in entropy. In biosynthesised adsorbent, cationic dye (Red 95) recovery for reprocessing was shown greatest in 0.1 M HCl. Thus, it determined that Red 95, a cationic dye, could be effectively removed from aqueous solution using biosynthesised adsorbent produced from cumnium cyminum.

Conflict of Interest:

The authors declare no conflict of interest.

Acknowledgement

The authors are grateful to KPR Institute of Engineering and Technology, Coimbatore, Tamil Nadu for providing facilities for the conduct of laboratory Investigations. The authors extend their appreciation to the Researchers Supporting Project number (RSP2023R396), King Saud University, Riyadh, Saudi Arabia.

References

Abrishamkar S., Mohammadi A., Vega L.D.J., Wang D. and Kalali N.E. (2023). Layer-by-layer assembly of calixarene modified GO and LDH nanostructures on flame retardancy, smoke suppression, and dye adsorption behavior of flexible polyurethane foams, *Polymer degradation and stability*, **207**, 110242.

Bensalah H., Bekheet F.M., Younssi A.S., Ouammou M. and Gurlo A. (2017). Removal of cationic and anionic textile dyes with Moroccan natural phosphate, *Journal of environmental chemical engineering*, **5**, 2189–2199.

Cui Z., Gan J., Xue Y., Zhang J., Zhang R., Liu J. and Hao J. (2019). Adsorption selectivity of cubic nano-CeO2 and effect of particle size on adsorption thermodynamics, *Fluid phase equilibria*, **502**, 112277.

Davarci D. and Zorlu Y.D.C. (2023). 3D Ag(I) coordination polymer constructed from a flexible pyridyloxycyclotetraphoshazene linker: Synthesis, crystal structure and dye adsorption properties, *Polyhedron*, **231**.116250.

Deluo Ji., Liu G., Zhang X., Zhang C. and Yuan S. (2019). Adsorption of C5Pe molecules on silica surfaces with different hydrophobicity studied by molecular dynamics simulation, *Applied surface science*, **495**, 143624.

Farhadi S., Amini M.M., Dusek M., Kucerakova M. and and Mahmoudi F. (2017). A new nanohybrid material constructed from Keggin-type polyoxometalate and Cd(II) semicarbazone Schiff base complex with excellent adsorption properties for the removal of cationic dye pollutants, *Journal of molecular structure*, **1130**, 592–602.

Gajera R., Patel V.R., Yadav A. and Labhasetwa K.P. (2022). Adsorption of cationic and anionic dyes on photocatalytic flyash/TiO2 modified chitosan biopolymer composite, *Journal of water processing Engineering*, **49**, 102993.

Gajera R., Patel V.R., Yadav A. and Labhasetwar K.P. (2022). Adsorption of cationic and anionic dyes on photocatalytic fly ash/TiO2 modified chitosan biopolymer composite, *Journal of water processing Engineering*, **49**, 102993.

Ghaemi N. and Safari P. (2018). Nano-porous SAPO-34 enhanced thin-film nanocomposite polymeric membrane: Simultaneously high-water permeation and complete removal of cationic/anionic dyes from water, *Journal of hazardous materials*, **358**, 376–388.

Gui Y., Chen J., Wang W., Zhu Y., Tang C. and Xu L. (2019). Adsorption mechanism of hydrogen sulfide and sulfur dioxide on Au–MoS2 monolayer, *Superlattices and microstructures*, **135**, 106280.

He Z., Qin M., Han C., Bai X., Wu , Yao D.D., Zheng Y. (2022). Pectin/graphene oxide aerogel with bamboo-like structure for enhanced dyes adsorption, *Colloids and surfaces A: Physicochemical and Engineering aspects*, **652**, 129837.

Hosseinzadeh.S., Hosseinzadeh.H., Pashaei S., and Khodaparast Z. (2018). Synthesis of magnetic functionalized MWCNT nanocomposite through surface RAFT co-polymerization of acrylic acid and N-isopropyl acrylamide for removal of cationic dyes from aqueous solutions, *Ecotoxicology and Environmental safety*, **161**, 34–44.

Hou Y., Yan S., Huang G., Yang Q., Huang S. and Jinjun Cai j. (2020). Fabrication of N-doped carbons from waste bamboo shoot shell with high removal efficiency of organic dyes from water, *Bioresource Technology*, **303**, 122939.

Huon M.T.D, Chai S.W, Show L.P, Lin Y, Chiu C., Tsai S. and Yu-KaungChang. (2020). Removal of cationic dye waste by nanofiber membrane immobilized with waste proteins, *International Journal of Biological Macromolecules*, **164**, 3873–3884.

Isanejad M., Arzani M., Mahdavi R.H. and Mohammadi T. (2017). Novel amine modification of ZIF-8 for improving simultaneous removal of cationic dyes from aqueous solutions using supported liquid membrane, *Journal of molecular liquids*, **225**, 800–809.

Janus R., Wadrzyk M., Natkanski P., Cool P., andKustrowski P. (2019). Dynamic adsorption–desorption of methyl ethyl ketone on MCM-41 and SBA-15 decorated with thermally activated polymers, *Journal of industrial and engineering chemistry*, **71**, 465–480.

Kadhom M., Albayati N., Alalwan H., and Al-Furaiji M. (2020). Removal of dyes by agricultural waste, *Sustainable chemistry and pharmacy*, **16**, 100259.

Kim S,. Kim D., Moradi H., Chang Y., and Yang J. (2023). Highly porous biobased graphene-like carbon adsorbent for dye removal: Preparation, adsorption mechanisms and optimization, *Journal of Environmental chemical Engineering*, **11**, 109278.

Kono H. (2017). Cationic flocculants derived from native cellulose: Preparation, biodegradability, and removal of dyes in aqueous solution, *Resource – Efficient Technologies*, **3**, 55–63.

Lapwanit S., Sooksimuang T. and Trakulsujaritchok T. (2018). Adsorptive removal of cationic methylene blue dye by kappa-carrageenan/poly(glycidyl methacrylate) hydrogel beads: Preparation and characterization, *Journal of environmental chemical engineering*, **5**, 6221–6230.

Li W., Bai Y., Ma Q., Chen W. and Hongzhu M H.W.M. (2018). Polyacrylic acid/CTAB-bentonite coated filter paper: Efficient and rapid removal of anionic and cationic dyes, *Applied surface science*, **458**, 903–909.

Li W., Ma Q., Bai Y., Xu D., Wu M., and Ma H. (2018). Facile fabrication of gelatin/bentonite composite beads for tunable removal of anionic and cationic dyes, *Chemical Engineering research and design*, **134**, 336–346.

Lin Y., Kao F., Chen S., Wey M., and Tseng H. (2020). A facile approach from waste to resource: Reclaimed rubber-derived membrane for dye removal", Journal of Taiwan institute of chemical Engineers, **112**, 286–295.

Liu A.M C., Omer, and Ouyang X. (2018). Adsorptive removal of cationic methylene blue dye using carboxymethyl cellulose/k-carrageenan/activated montmorillonite composite beads: Isotherm and kinetic studies, *International Journal of biological macromolecules*, **106**, 823–833.

Lv H.W., Jiang H, Fu-An H, Hu Q, Zhong Z, and Yang Y. (2022). Adsorption of anionic and cationic dyes by a novel crosslinked cellulose-tetrafluoroterephthalonitrile-tannin polymer, *European Polymer Journal*, **180**, 111602.

Ma C, Jin W, Ma X, Han H, Yu J, Wu Y. (2019). Water adsorption behaviors of high index polar surfaces in ZnO, *Applied surface science*, **498**, 143898.

Hasanpour M. and Hatami M. (2020). Photocatalytic performance of aerogels for organic dyes removal from wastewaters: Review study", Journal of molecular liquids, Volume.309, 113094.

Nasiri R, and Arsalani N. (2018). Synthesis and application of 3D graphene nanocomposite for the removal of cationic dyes from aqueous solutions: Response surface methodology design, *Journal of cleaner production*, **190**, .63–71.

Nayunigari M.K., Das R., Maity A., Agarwal S. and Vinod Kumar Gupta V.K. (2017). Folic acid modified cross-linked cationic polymer: Synthesis, characterization and application of the removal of Congo red dye from aqueous medium, *Journal of molecular liquid*, **227**, 87–97.

Pradhan K.S.S., Konwar T.N., Ghosh B., Mondal S.K. and Deb P.S. (2020). "Multifunctional Iron oxide embedded reduced graphene oxide as a versatile adsorbent candidate for

effectual arsenic and dye removal, *Colloid and interface science communications*, **39**, 100319.

Priya, Sharma A.K., Kaith S.B, Chandel K, Vipula, Isha AnoopSingh I. (2020). Bifunctional gelatin/dextrin hybrid backbone based fluorescent chemo-sensor for the detection of tannic acid and removal of eosin yellow dye, *Materials chemistry and physics*, **254**, 123304.

Qingwen L, Kewang W, Mengfan G, Yunshan B, Lei C, and Hongzhu M. (2017). Effectively removal of cationic and anionic dyes by pH-sensitive amphoteric adsorbent derived from agricultural waste-wheat straw, *Journal of Taiwan institute of chemical engineers*, **76**, 65–72.

Senoussi H., and Bouhidel K. (2018). Feasibility and optimisation of a batch mode capacitive deionization (BM CDI) process for textile cationic dyes (TCD) removal and recovery from industrial wastewaters, *Journal of cleaner production*, 205, 721–727.

Shi Y, Liu G, Wang L, and Zhang H. (2019). Heteroatom-doped porous carbons from sucrose and phytic acid for adsorptive desulfurization and sulfamethoxazole removal: A comparison between aqueous and non-aqueous adsorption, *journal of colloid and interface science*, **557**, 336–348.

Shimizu K.T., Kanishka H., Silva D, Hara M, and Yoshimura M. (2022). Facile synthesis of carbon nanotubes and cellulose nanofiber incorporated graphene aerogels for selective organic dye adsorption, *Applied surface sciences*, **600**, 154098.

Soni S, Bajpai P.K, Mittal J, and Arora C. (2020). Utilisation of cobalt doped Iron based MOF for enhanced removal and recovery of methylene blue dye from wastewater, *Journal of molecular liquids*, 113642.

Vahedi S, Tavakoli O, Khoobi M, Ansari A, and Faramarzi A.M. (2017). Application of novel magnetic β-cyclodextrin-anhydride polymer nano-adsorbent in cationic dye removal from aqueous solution, *Journal of Taiwan institute of chemical engineers*, **80**, 452–463.

Wang F, Huang K, Xu Z, Cao F, Chen C, Shi F, Chen N. (2022). "Preparation of high-strength dynamic polysaccharide nanocomposite hydrogels and their application towards dye adsorption, *Industrial crops and products*, **189**, 115704.

Wang G, Wang S, Sun W, Sun Z, and Zheng S. (2017). Oxygen functionalized carbon nanocomposite derived from natural illite as adsorbent for removal of cationic and anionic dyes, *Advanced powder technology*, **28**, 1943–1953.

Wang N, Liu H, Kang C, Wang Y, Kunkun X, and Tian T. (2019). Removal of γ-HCH, 1,4-Dichlorobenzene and trichloromethane from air via the adsorption of snow, *Atmospheric Environment*, **213**, 377–383.

Wang R.F, Deng L, Li K, Fan X, Li W, and Lu H. (2020). Fabrication and characterization of sugarcane bagasse–calcium carbonate composite for the efficient removal of crystal violet dye from wastewater, *Ceramics international*, **46**, 27484–27492.

Wang Y, Du T, Jia H, Qiu Z, and Song Y. (2019). Effect of extra-framework cation in ion-exchanged ZSM-5 from rice husk ash on CO2 adsorption, *Solid state sciences*, **97**, 105958.

Wu S, Deng C, and Wang X. (2019). Molecular simulation of flue gas and CH4 competitive adsorption in dry and wet coal, *Journal of natural gas sciences and engineering*, **71**, 102980.

Xu M, Bi B, Xu B, Sun Z, and Xu L. (2018). Polyoxometalate-intercalated ZnAlFe-layered double hydroxides for adsorbing removal and photocatalytic degradation of cationic dye, *Applied clay science*, **157**, 86–91.

Xu W, Chen Y, Zhang W, and Li B.B. (2019). Fabrication of graphene oxide/bentonite composites with excellent adsorption performances for toluidine blue removal from aqueous solution, *Advanced powder technology*, **30**, 493–501.

Yang C, Xu W., Nan Y, Wang Y, and Chen X.X. (2020). Novel negatively charged nanofiltration membrane based on 4,4'-diaminodiphenylmethane for dye removal, *Separation and purification technology*, **248**, 117089.

Yang Q, Lu R, Ren S.S, Chen C, Chen Z, and Yang X. (2018). Three-dimensional reduced graphene oxide/ZIF-67 aerogel: Effective removal cationic and anionic dyes from water, *Chemical engineering journal*, **348**, 202–211.

Yao Y.D.Y, and Ameta R.K. (2023). Removal and recovering of anionic and cationic dyes using Neem Leaf ash prepared at 250, 500 and 750 °C: Analyzed by adsorption isotherm and physicochemical parameters, *Journal of molecular liquids*, **370**, 121012.

Yu W, Xu H, Roden E.E, and Wan Q. (2019). Efficient adsorption of iodide from water by chrysotile bundles with wedge-shaped nanopores, *Applied clay science*, **183**, 105331.

Yuan Y, Dong X., and Ricardez-Sandoval L. (2019). A density functional theory analysis on syngas adsorption on NiO (100) surface, *Applied surface science*, **498**,143782.

Yun J, Wang Y, Liu Z, Li Y, Yang H, and Xu Z. (2020). High efficient dye removal with hydrolyzed ethanolamine-Polyacrylonitrile UF membrane: Rejection of anionic dye and selective adsorption of cationic dye, Chemosphere, **259**, 127390.

Zereshki S, Daraei P, Shokri A. (2018). Application of edible paraffin oil for cationic dye removal from water using emulsion liquid membrane, *Journal of hazardous materials*, **356**, 1–8.

Zhang L, Zhang H, Guo W., and Tian Y. (2014). Removal of malachite green and crystal violet cationic dyes from aqueous solution using activated sintering process red mud, *Applied clay science*, 93–94, 85–93.

Zhiming S, Guangyuan Y, Mingyi L, and Shuilin Z. (2017). In situ synthesis of magnetic MnFe2O4/diatomite nanocomposite adsorbent and its efficient removal of cationic dyes, *Journal of Taiwan institute of chemical engineers*, **71**, 501–509.

Zhou Y, Hu Y, Huang W, Cheng G, Cui C, and Lu J. (2018). A novel amphoteric β-cyclodextrin-based adsorbent for simultaneous removal of cationic/anionic dyes and bisphenol A, *Chemical engineering journal*, **341**, .47–57.

Zhu H., Chen S., Duan H., He J., and Luo Y. (2023). Removal of anionic and cationic dyes using porous chitosan/carboxymethyl cellulose-PEG hydrogels: Optimization, adsorption kinetics, isotherm and thermodynamics studies, *International Journal of Biological macromolecules*, Available online **11**, 123213.